

This work was written as part of one of the author's official duties as an Employee of the United States Government and is therefore a work of the United States Government. In accordance with 17 U.S.C. 105, no copyright protection is available for such works under U.S. Law.

Public Domain Mark 1.0

<https://creativecommons.org/publicdomain/mark/1.0/>

Access to this work was provided by the University of Maryland, Baltimore County (UMBC) ScholarWorks@UMBC digital repository on the Maryland Shared Open Access (MD-SOAR) platform.

Please provide feedback

Please support the ScholarWorks@UMBC repository by emailing scholarworks-group@umbc.edu and telling us what having access to this work means to you and why it's important to you. Thank you.

Progress on Ultra-Heavy Cosmic-Ray Analysis with CALET on the International Space Station

Wolfgang V. Zober,^{†,a,*} Brian F. Rauch,^a Anthony W. Ficklin^b and Nicholas Cannady^c on behalf of the CALET Collaboration

(a complete list of authors can be found at the end of the proceedings)

^a*Department of Physics and McDonnell Center for the Space Sciences, Washington University, St. Louis, MO 63130 USA*

^b*Department of Physics and Astronomy, Louisiana State University, Baton Rouge, LA 70803 USA*

^c*CRESST-II/University of Maryland, Baltimore County/NASA Goddard Space Flight Center*
E-mail: wzober@wustl.edu

The Calorimetric Electron Telescope (CALET), launched to the International Space Station in August 2015 and continuously operating since, measures cosmic-ray (CR) electrons, nuclei and gamma-rays. CALET utilizes its main calorimeter charge detector to measure CR nuclei from ${}^1\text{H}$ to ${}_{40}\text{Zr}$. In order to maximize the acceptance of the rare ultra-heavy (UH) CR above ${}_{30}\text{Zn}$, a special high duty cycle ($\sim 90\%$) UH trigger is used that does not require passage through the 27 radiation length deep Total Absorption Calorimeter (TASC). This provides a $6\times$ increase in geometry factor allowing CALET to collect in 5 years a UHCR dataset with statistics comparable to those from the first flight of the balloon-borne SuperTIGER instrument but without the need for atmospheric corrections. Previous CALET UHCR analyses using time and position corrections based on ${}_{26}\text{Fe}$ and a geomagnetic vertical cutoff rigidity selection have shown abundances of even nuclei in agreement with SuperTIGER. To further improve resolution and maximize statistics, a trajectory dependent geomagnetic rigidity selection has been employed here with further work being done to implement a Cash-Karp Runge-Kutta ray tracing method for an improved determination of effective cutoff rigidities. Additional work has also been done to analyze events from the smaller dataset of events that pass through the TASC, which provides energy information and a better charge assignment that will provide higher resolution UH measurements, albeit with lower statistics.

37th International Cosmic Ray Conference (ICRC 2021)

July 12th – 23rd, 2021

Online – Berlin, Germany

*Presenter

[†]CALET supported by JAXA in Japan, ASI in Italy, and in the USA by NASA grant # NNX16AC02G and 80NSSC20K0399 at WUSTL, 4-APRA14-0075 at GSFC and NNX16AB99G at LSU

1. Introduction

The CALorimetric Electron Telescope (CALET) on the International Space Station (ISS) is a Japanese led astroparticle observatory that was launched on August 19, 2015 and has been collecting scientific data since October 13, 2015 [1]. As its name suggests, the main science objective of CALET is to directly measure the total cosmic-ray electron flux ($e^- + e^+$) to the highest energies (1 GeV to 20 TeV) [2–6] with the main calorimeter (CAL), shown in the CALET instrument package in Fig. 1a. The calorimeter is also capable of measuring gamma rays (10 GeV to 10 TeV) [7–9] and cosmic-ray nuclei (up to 1,000 TeV) [10–14]. In addition, there is the CALET Gamma-ray Burst Monitor (CGBM) [9], which can make simultaneous observations with the calorimeter.

The main calorimeter instrument is comprised of three detector systems, shown in more detail in a side view in Fig. 1b. At the top is the charge detector (CHD), comprised of an x and a y layer, each having 14 scintillator paddles. The paddles all are 32 mm wide by 10 mm thick by 450 mm long. Below the CHD is the imaging calorimeter (IMC), which is 156.5 mm tall, and made of 8 layers of both x and y scintillating fibers that are 1 mm wide squares and 448 mm long. In between the fiber layers of the IMC are a combined 3.0 radiation lengths (X_0) of tungsten arranged such that the first 5 layers are $0.2X_0$ thick and the bottom two are each $1.0X_0$ thick. At the bottom of the instrument stack is the total absorption calorimeter (TASC). This is made of 6 x and y layers of 16 lead tungstate (PWO) scintillator logs. Each of these logs are 19 mm wide, 20 mm tall, and 326 mm long. Combined these logs give the TASC a depth of $27X_0$.

The CHD, along with the IMC, provides the primary particle charge identification. All three detectors are utilized for track reconstruction, but that is primarily based on the IMC, while the particle energy is determined from the calorimeters, with most of the determination based on TASC measurements.

2. Ultra-Heavy Cosmic Rays

The measurement of ultra-heavy cosmic rays (UHCN), $_{30}\text{Zn}$ and higher charge elements, provides insight into the origins of cosmic rays. In Fig. 2, the relative abundances of elements ($1 \leq$

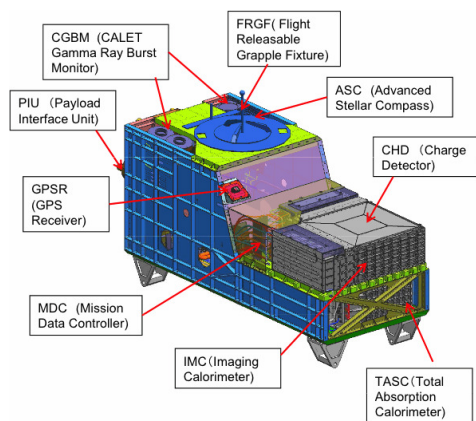


Figure 1(a): CALET instrument package detailing locations of the various CALET subsystems.

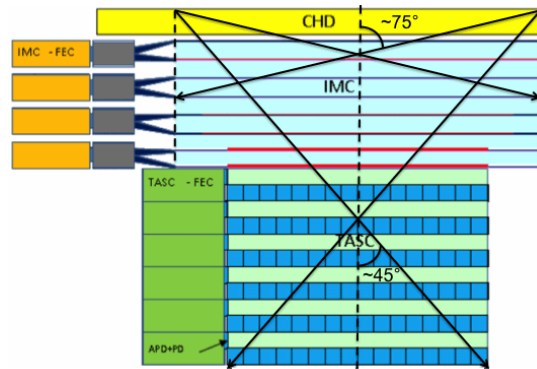


Figure 1(b): CALET side-view showing CHD, IMC, and TASC detector placement with the maximum acceptance angles for detection. For the UH trigger analysis this is 75° and in the TASC analysis this is 45° .

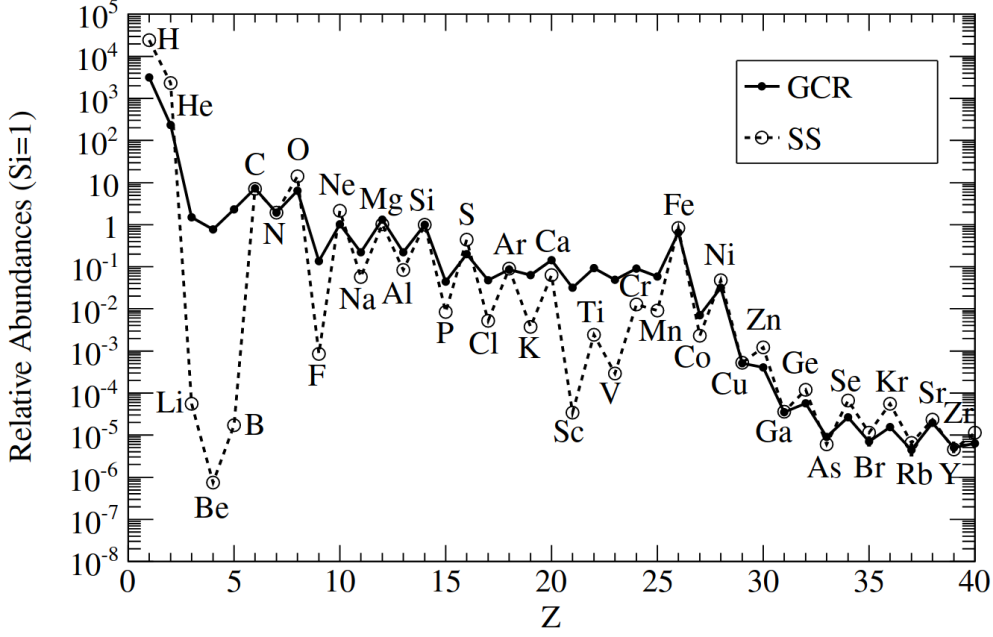


Figure 2: Solar System (SS) [19] and Galactic cosmic-ray (GCR) relative abundances at 2 GeV/nuc. GCR data is sourced for $1 \leq Z \leq 2$ from [20], $Z = 3$ from [21], $4 \leq Z \leq 28$ from [22], $Z = 29$ from [15], and $28 \leq Z \leq 40$ from [16] and normalized to ${}_{14}\text{Si}$.

$Z \leq 40$) for cosmic rays with energies of 2 GeV/nucleon are compared with the Solar System (SS) abundances normalized to ${}_{14}\text{Si}$. These two samples of galactic matter are nominally consistent, with most of the differences accounted for through both cosmic ray spallation between source and detection and by acceleration efficiencies. In the cosmic rays we see that ${}_{26}\text{Fe}$ is $\sim 5 \times 10^3$ times less abundant than ${}_{1}\text{H}$, and that the UHCR with charges $30 \leq Z \leq 40$ are $\sim 10^5$ times less abundant than ${}_{26}\text{Fe}$. Single-element resolution UHCR measurements have so far only been made up to ${}_{40}\text{Zr}$ by the TIGER [15] and made up to ${}_{56}\text{Ba}$ by SuperTIGER [17] balloon-borne instruments at GeV/nuc energies, and up to ${}_{40}\text{Zr}$ by the ACE-CRIS [18] space based instrument at hundreds of MeV/nuc. The UHCR composition shows enhancement in material produced in massive stars, both from stellar outflows during the stars' lives and in the ejecta from supernova. This suggests that a significant fraction of the cosmic rays originate in OB associations, which is where the majority of supernovae that are believed to accelerate the galactic cosmic rays occur. The fact that the cosmic-ray source appears to be enhanced in massive star material compared to SS would suggest that UHCR observations can help constrain the relative contributions of supernovae and binary neutron star mergers to the heavy r-process elements.

CALET observations will contribute to the statistics of the UHCR data set and complement other existing measurements. The ultra-heavy (UH) event trigger on CALET, which requires events only pass through the CHD and top half of the IMC, after 5 years collected UHCR statistics similar to those achieved in the first flight of the balloon-borne SuperTIGER instrument. CALET also observes a similar energy range to TIGER and SuperTIGER, but requires corrections for different systematic effects. The balloon based observations must be corrected for energy losses and nuclear interactions that occur in the atmosphere, while ISS based measurements are subject to screening

by Earth's geomagnetic field. Comparatively, UHCR observations made by ACE-CRIS occur outside the geomagnetic field in a complementary lower energy range. So while ACE-CRIS and SuperTIGER instruments only measure down to ${}_5\text{B}$ and ${}_{10}\text{Ne}$, respectively, CALET has measured cosmic-ray abundances in the $1 \leq Z \leq 40$ charge range providing complementary measurements, and a check of the cross calibrations of other instruments.

3. Analysis

3.1 Previous Results

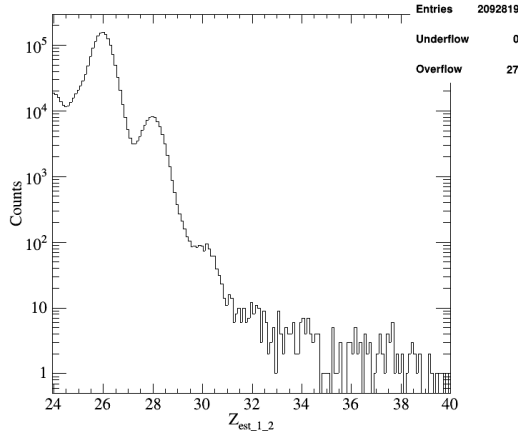


Figure 3(a): 2019 ICRC results of the UH trigger analysis, bin size in 0.1 units of charge.

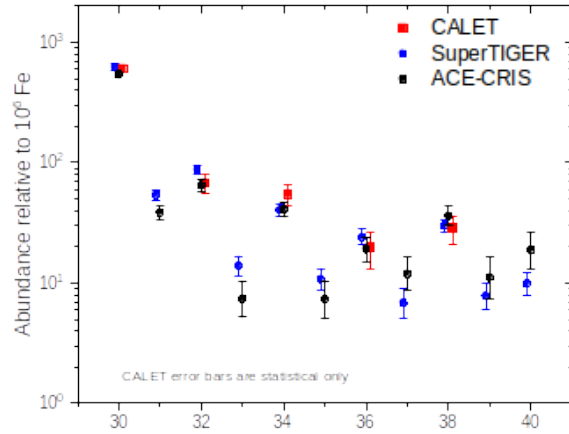


Figure 3(b): Comparison of CALET to SuperTIGER and ACE-CRIS.

Preliminary CALET UHCR results for the even elements reported at the previous ICRC were consistent with those published for SuperTIGER [17] (Fig. 3b). That analysis was based on ~ 34 months of data collected by CALET's ultra-heavy trigger, which provides an increased acceptance by requiring an event trajectory only passes through the CHD and the top half of the IMC (Fig. 1b). This has an acceptance angle of 75° , which gives a geometry factor of $0.44 \text{ m}^2\text{sr}$. The UH-trigger analysis then used a $\theta \leq 45^\circ$ incidence angle cut selection with a minimum signal threshold from the top four layers of the IMC and a minimum geomagnetic vertical cutoff rigidity of 4 GV (Fig. 3a).

In addition, there are time response corrections for CALET based on the signal response from ${}_{26}\text{Fe}$ events. For each CHD paddle the ${}_{26}\text{Fe}$ peak is fit in time intervals selected such that there is a minimum of ~ 500 events in each peak. Paddle correction factors are derived by dividing the mean ${}_{26}\text{Fe}$ peak position of all paddles in the data set by the time dependent paddle means. The position corrections look at both the ${}_{14}\text{Si}$ and ${}_{26}\text{Fe}$ mean fits. In this position correction each CHD paddle is divided along their length into 42 segments that are $\sim 1/3$ the width of the paddles, with each segment normalized by linearly scaling ${}_{14}\text{Si}$ and ${}_{26}\text{Fe}$ mean fits.

3.2 Rigidity Methods

Since that ICRC, a model for the geomagnetic field has been implemented that provides the field strength as a function of time, latitude, longitude, and altitude, and then takes in the angle of detection in the frame of the Earth's magnetosphere to provide an angle-dependent minimum

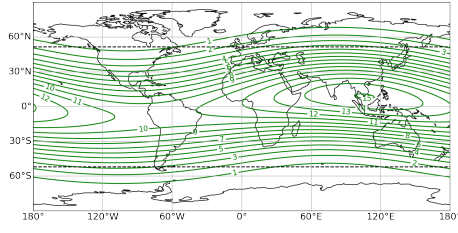


Figure 4(a): Vertical cutoff rigidity (GV) based on current IGRF-13 values at the ISS altitude of 400 km overlaid the region of ISS transit.

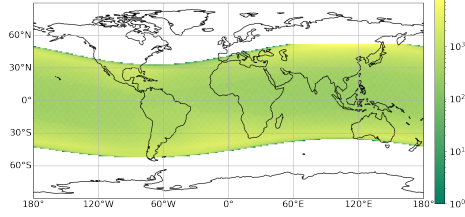


Figure 4(b): UH events as seen by CALET with a time-dependent calculated angle dependent rigidity value ≥ 4 GV.

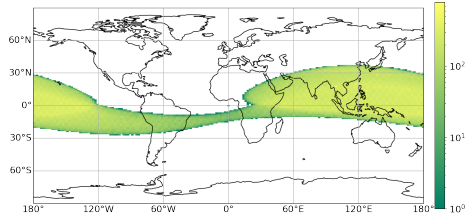


Figure 4(c): UH events as seen by CALET with a time-dependent calculated angle dependent rigidity value ≥ 12 GV.

rigidity for all CALET UH events. This angle dependant minimum rigidity is based on the Störmer approximation (Equation 1). This method allows for a more refined selection than with just the vertical cutoff rigidity.

$$P \geq \frac{1}{r^2} C_S \left(\frac{1 - \sqrt{1 - \cos \gamma \cos^3 \lambda}}{\cos \gamma \cos \lambda} \right)^2 \quad (1)$$

Where λ is the magnetic latitude, r is the distance from Earth's center, γ is the east-west inclination, and C_S is the Störmer constant which is derived from the magnetic dipole moment. The vertical case, where γ is 90° , is shown in Fig.4a. By comparison, Fig.4b and Fig.4c show actual event locations for different minimum rigidities. In Fig.4b, which shows all UH-trigger events with rigidity greater than 4 GV, one sees that event region does not differ much from vertical, but at higher rigidities (Fig. 4c: ≥ 12 GV) the effect of East-West angle becomes more apparent. These calculated rigidity values are then used in the overall UH-trigger analysis (Fig. 5a). Also along these lines, there has been development on determining the effective cutoff rigidity by tracing each UH-trigger event trajectory in a complete geomagnetic field model that includes solar effects to more precisely determine its geomagnetic threshold.

Simultaneous to the work shown in this section, a complementary analysis based on determining rigidity via L-shells rather than the Störmer approximation, together with a new ray-tracing algorithm, can be found in ref [24]. The effects these methods have on the UH abundances are shown in the histograms in Figs. 5a and 5b.

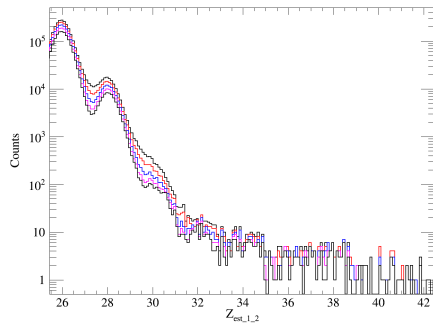


Figure 5(a): Variation in Z due to different minimum cutoff rigidity, bin size in 0.1 units of charge. Minimum cutoff rigidity ranges from 2-4 GV with 2.5 GV in red, 3 GV in blue, and 3.5 GV in purple.

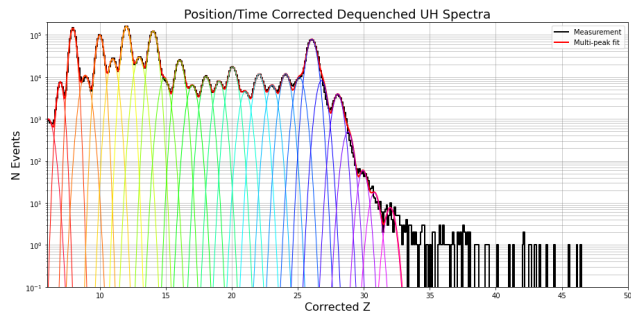


Figure 5(b): Charge histogram produced through L-Shell determination of rigidity. Minimum rigidity threshold of 4 GV bin size in 0.1 units of charge.

3.3 TASC analysis

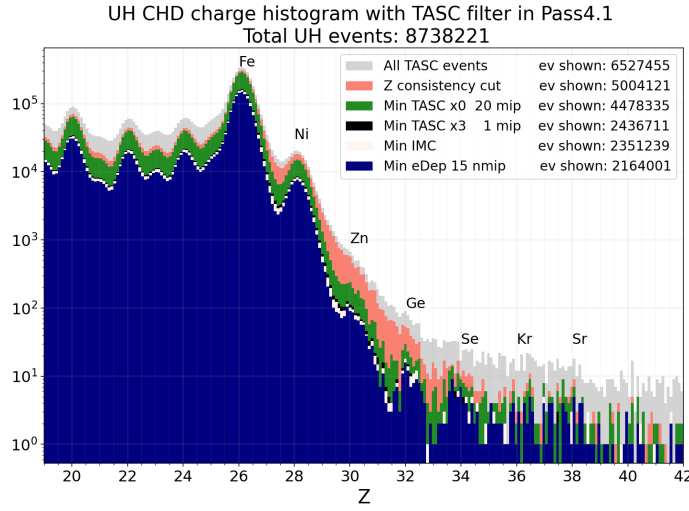


Figure 6: A charge histogram showing what each successive cut on the TASC data-set does step-by-step from a charge consistency cut that requires both x and y layers to be within 2.00%, cuts on multiple layers of the TASC and IMC, as well as a minimum TASC energy.

are then determined by a multiple-Gaussian fit with integer charge means shown in Fig. 7a. By comparison with the histograms in Figs. 5a and 5b, you can see that there is an improved resolution of higher charge peaks without much of a loss in statistics, and in Fig. 7b the odd-even pairs ($_{27}\text{Co}$ & $_{28}\text{Ni}$, $_{29}\text{Cu}$ & $_{30}\text{Zn}$, etc.) of relative abundances are compared to both ACE-CRIS's preliminary top-of-instrument [18] and SuperTIGER's top-of-atmosphere abundances [26]. Future work on this will incorporate time and position corrections similar to the those done for the CHD in the UH-trigger analysis and do a charge assignment by bins of deposited energy in the TASC.

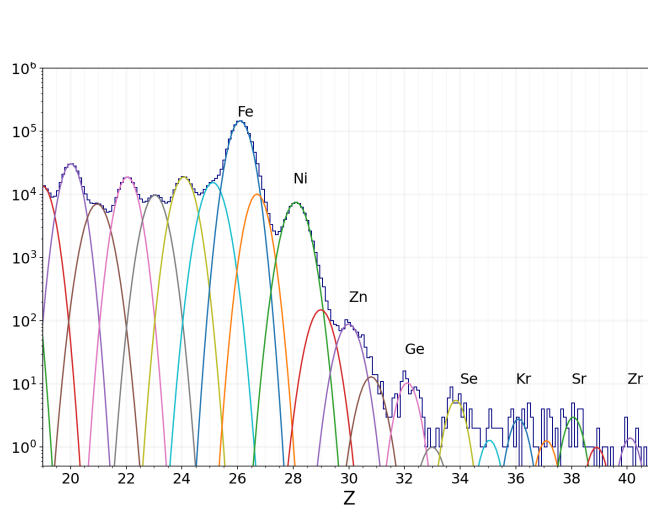


Figure 7(a): UHCR TASC analysis histogram with multiple gaussian fitting, bin size in 0.1 units of charge.

Since the last ICRC, work has been done to construct a complementary analysis with the data set of events that pass through the TASC with the 45° acceptance angle shown in Fig. 1b, which provides each event with an energy. In this analysis cuts are done for a minimum energy on the top layer and in the middle of the TASC. There is a further requirement on minimum total energy deposited based on the assigned charge. Additionally, there is a charge consistency cut requiring that the calculated CHD charge for both x and y layers is within 2.00%. The successive effects of these cuts are shown in Fig. 6.

A Tarle model charge assignment [25] is done and the abundances

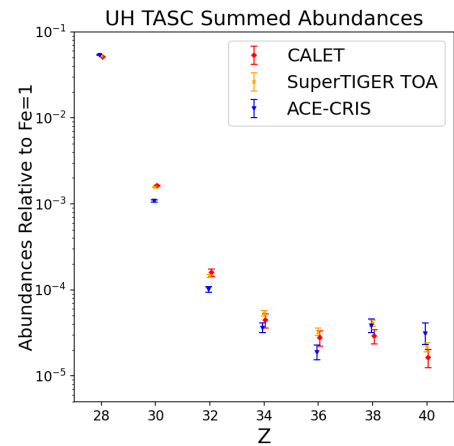


Figure 7(b): Comparison of the relative abundances of the summed odd-even pairs with SuperTIGER[26] and ACE-CRIS[18] for Z between $27 \leq Z \leq 40$. Errors bars are statistical only.

4. Conclusions

Preliminary abundances from CALET UH-trigger and TASC UHCR analyses continue to agree with previous CALET results and other instrument measurements. CALET continues to output excellent data from the International Space Station, and it is expected to continue operating for several more years. This further data-collection will allow improved statistics for CALET to contribute to the total UHCR data set, and complement the measurements made by other balloon and space-borne instruments.

Acknowledgements

The material contained in this document is based upon work supported by a National Aeronautics and Space Administration (NASA) grant or cooperative agreement. Any opinions, findings, conclusions, or recommendations expressed in this material are those of the author and do not necessarily reflect the views of NASA.

References

- [1] P.S. Marrocchesi for the CALET Collaboration, *New Results from the first 5 years of CALET observations on the International Space Station*, in proceedings of *The 37th International Cosmic Ray Conference*, PoS (ICRC2021) 010 (2021)
- [2] S. Torii and Y. Akaike for the CALET Collaboration, *Precise Measurement of the Cosmic-Ray Electron and Positron Spectrum with CALET on the International Space Station*, in proceedings of *The 37th International Cosmic Ray Conference*, PoS (ICRC2021) 105 (2021)
- [3] E. Berti for the CALET Collaboration, *The analysis strategy for the measurement of the electron flux with CALET on the International Space Station*, in proceedings of *The 37th International Cosmic Ray Conference*, PoS (ICRC2021) 065 (2021)
- [4] A. Bruno, G. A. de Nolfo, A. Ficklin et. al. for the CALET Collaboration, *Relativistic Electron Precipitation Observations with CALET on the International Space Station*, in proceedings of *The 37th International Cosmic Ray Conference*, PoS (ICRC2021) 1295 (2021)
- [5] H. Motz for the CALET Collaboration, *Investigating the Vela SNR's Emission of Electron Cosmic Rays with CALET at the International Space Station*, in proceedings of *The 37th International Cosmic Ray Conference*, PoS (ICRC2021) 100 (2021)
- [6] S. Miyake for the CALET Collaboration, *Solar Modulation During the Descending Phase of Solar Cycle 24 Observed with CALET on the International Space Station*, in proceedings of *The 37th International Cosmic Ray Conference*, PoS (ICRC2021) 1270 (2021)
- [7] M. Mori for the CALET Collaboration, *High-energy gamma-ray observations above 10 GeV with CALET on the International Space Station*, in proceedings of *The 37th International Cosmic Ray Conference*, PoS (ICRC2021) 619 (2021)
- [8] N. Cannady for the CALET Collaboration, *Low-energy gamma-ray observations above 1 GeV with CALET on the International Space Station*, in proceedings of *The 37th International Cosmic Ray Conference*, PoS (ICRC2021) 604 (2021)
- [9] Y. Kawakubo for the CALET Collaboration, *Gamma-ray burst observation & gravitational wave event follow-up with CALET on the International Space Station*, in proceedings of *The 37th International Cosmic Ray Conference*, PoS (ICRC2021) 957 (2021)

- [10] K. Kobayashi for the CALET Collaboration, *Extended measurement of the proton spectrum with CALET on the International Space Station*, in proceedings of *The 37th International Cosmic Ray Conference*, PoS (ICRC2021) 098 (2021)
- [11] Y. Akaïke and P. Maestro for the CALET Collaboration, *Measurement of the cosmic-ray secondary-to-primary ratios with CALET on the International Space Station*, in proceedings of *The 37th International Cosmic Ray Conference*, PoS (ICRC2021) 112 (2021)
- [12] P. Brogi for the CALET Collaboration, *Measurement of the energy spectrum of cosmic-ray helium with CALET on the International Space Station*, in proceedings of *The 37th International Cosmic Ray Conference*, PoS (ICRC2021) 101 (2021)
- [13] P. Maestro for the CALET Collaboration, *Energy spectra of carbon and oxygen cosmic rays with CALET on the International Space Station*, in proceedings of *The 37th International Cosmic Ray Conference*, PoS (ICRC2021) 093 (2021)
- [14] F. Stolzi, C. Checchia, and Y. Akaïke for the CALET Collaboration, *Measurement of the iron spectrum with CALET on the International Space Station*, in proceedings of *The 37th International Cosmic Ray Conference*, PoS (ICRC2021) 109 (2021)
- [15] B.F. Rauch et al., *Cosmic Ray origin in OB Associations and Preferential Acceleration of Refractory Elements: Evidence from Abundances of Elements ^{26}Fe through ^{34}Se* , ApJ, 697(2009) 2083-2088, [arXiv:0906.2021](#)
- [16] R.P. Murphy et al., *Galactic Cosmic Ray Origins and OB Associations: Evidence from SuperTIGER Observations of Elements ^{26}Fe Through ^{40}Zr* , ApJ, 831(2016) 2083-2088, [arXiv:1608.08183](#).
- [17] N. Walsh et. al, *SuperTIGER abundances of galactic cosmic rays for the charge interval $41 \leq Z \leq 56$* , Advances in Space Research (pending)
- [18] W.R. Binns, M.H. Israel, M.E. Wiedenbeck, et al., *Elemental Source Composition Measurements and the Origin of Galactic Cosmic Rays - ACE-CRIS Observations of UH Elements*, in proceedings of *The 36th International Cosmic Ray Conference*, PoS (ICRC2021) 673 (2019)
- [19] K. Lodders, *Solar System Abundances and Condensation Temperatures of the Elements*, ApJ, 591(2003) 1220-1247.
- [20] T. Sanuki et al., *Precise Measurement of Cosmic-Ray Proton and Helium Spectra with the BESS Spectrometer*, ApJ, 545(2000) 148-155, [arXiv:astro-ph/0002481](#).
- [21] M. Aguilar et al., *Isotopic Composition of Light Nuclei in Cosmic Rays: Results from AMS-01*, ApJ, 736(2011), 105-116, [arXiv:1106.2269](#)
- [22] J.J. Engelmann et al., *Charge composition and energy spectra of cosmic-ray nuclei for elements from Be to Ni - Results from HEAO-3-C2*, A&A, 233(1990), 96-111
- [23] B.F. Rauch and W.R. Binns for the CALET Collaboration, *CALET Ultra Heavy Cosmic Ray Observations on the ISS*, in proceedings of *The 36th International Cosmic Ray Conference*, PoS (ICRC2021) 130 (2019)
- [24] A. Ficklin, N. Cannady, B. F. Rauch, W. V. Zober et. al for the CALET Collaboration, *Ultra-Heavy Cosmic Ray Analysis with CALET on the International Space Station: Established and Developing Procedures*, in proceedings of *The 37th International Cosmic Ray Conference*, PoS (ICRC2021) 069 (2021)
- [25] G. Tarle, S. P. Ahlen, and B. G. Cartwright. *Cosmic Ray Isotope Abundances from Chromium to Nickel*. ApJ, 230(1979), 607–620.
- [26] N. Walsh *SuperTiger Elemental Abundances for the Charge Range $41 \leq Z \leq 56$* (Doctoral dissertation, Washington University in St. Louis). (2020)

Full Authors List: CALET Collaboration

O. Adriani^{1,2}, Y. Akaike^{3,4}, K. Asano⁵, Y. Asaoka⁵, E. Berti^{1,2}, G. Bigongiari^{6,7}, W. R. Binns⁸, M. Bongi^{1,2}, P. Brogi^{6,7}, A. Bruno^{9,10}, J. H. Buckley⁸, N. Cannady^{11,12,13}, G. Castellini¹⁴, C. Checchia⁶, M. L. Cherry¹⁵, G. Collazuol^{16,17}, K. Ebisawa¹⁸, A. W. Ficklin¹⁵, H. Fuke¹⁸, S. Gonzi^{1,2}, T. G. Guzik¹⁵, T. Hams¹¹, K. Hibino¹⁹, M. Ichimura²⁰, K. Ioka²¹, W. Ishizaki⁵, M. H. Israel⁸, K. Kasahara²², J. Kataoka²³, R. Kataoka²⁴, Y. Katayose²⁵, C. Kato²⁶, N. Kawanaka^{27,28}, Y. Kawakubo¹⁵, K. Kobayashi^{3,4}, K. Kohri²⁹, H. S. Krawczynski⁸, J. F. Krizmanic^{11,12,13}, P. Maestro^{6,7}, P. S. Marrocchesi^{6,7}, A. M. Messineo^{30,7}, J.W. Mitchell¹², S. Miyake³², A. A. Moiseev^{33,12,13}, M. Mori³⁴, N. Mori², H. M. Motz³⁵, K. Munakata²⁶, S. Nakahira¹⁸, J. Nishimura¹⁸, G. A. de Nolfo⁹, S. Okuno¹⁹, J. F. Ormes³⁶, N. Ospina^{16,17}, S. Ozawa³⁷, L. Pacini^{1,14,2}, P. Papini², B. F. Rauch⁸, S. B. Ricciarini^{14,2}, K. Sakai^{11,12,13}, T. Sakamoto³⁸, M. Sasaki^{33,12,13}, Y. Shimizu¹⁹, A. Shiomi³⁹, P. Spillantini¹, F. Stolzi^{6,7}, S. Sugita³⁸, A. Sulaj^{6,7}, M. Takita⁵, T. Tamura¹⁹, T. Terasawa⁴⁰, S. Torii³, Y. Tsunesada⁴¹, Y. Uchihori⁴², E. Vannuccini², J. P. Wefel¹⁵, K. Yamaoka⁴³, S. Yanagita⁴⁴, A. Yoshida³⁸, K. Yoshida²², and W. V. Zober⁸

¹Department of Physics, University of Florence, Via Sansone, 1, 50019 Sesto, Fiorentino, Italy, ²INFN Sezione di Florence, Via Sansone, 1, 50019 Sesto, Fiorentino, Italy, ³Waseda Research Institute for Science and Engineering, Waseda University, 17 Kikuicho, Shinjuku, Tokyo 162-0044, Japan, ⁴JEM Utilization Center, Human Spaceflight Technology Directorate, Japan Aerospace Exploration Agency, 2-1-1 Sengen, Tsukuba, Ibaraki 305-8505, Japan, ⁵Institute for Cosmic Ray Research, The University of Tokyo, 5-1-5 Kashiwa-no-Ha, Kashiwa, Chiba 277-8582, Japan, ⁶Department of Physical Sciences, Earth and Environment, University of Siena, via Roma 56, 53100 Siena, Italy, ⁷INFN Sezione di Pisa, Polo Fibonacci, Largo B. Pontecorvo, 3, 56127 Pisa, Italy, ⁸Department of Physics and McDonnell Center for the Space Sciences, Washington University, One Brookings Drive, St. Louis, Missouri 63130-4899, USA, ⁹Heliospheric Physics Laboratory, NASA/GSFC, Greenbelt, Maryland 20771, USA, ¹⁰Department of Physics, Catholic University of America, Washington, DC 20064, USA, ¹¹Center for Space Sciences and Technology, University of Maryland, Baltimore County, 1000 Hilltop Circle, Baltimore, Maryland 21250, USA, ¹²Astroparticle Physics Laboratory, NASA/GSFC, Greenbelt, Maryland 20771, USA, ¹³Center for Research and Exploration in Space Sciences and Technology, NASA/GSFC, Greenbelt, Maryland 20771, USA, ¹⁴Institute of Applied Physics (IFAC), National Research Council (CNR), Via Madonna del Piano, 10, 50019 Sesto, Fiorentino, Italy, ¹⁵Department of Physics and Astronomy, Louisiana State University, 202 Nicholson Hall, Baton Rouge, Louisiana 70803, USA, ¹⁶Department of Physics and Astronomy, University of Padova, Via Marzolo, 8, 35131 Padova, Italy, ¹⁷INFN Sezione di Padova, Via Marzolo, 8, 35131 Padova, Italy, ¹⁸Institute of Space and Astronautical Science, Japan Aerospace Exploration Agency, 3-1-1 Yoshinodai, Chuo, Sagami-hara, Kanagawa 252-5210, Japan, ¹⁹Kanagawa University, 3-27-1 Rokkakubashi, Kanagawa, Yokohama, Kanagawa 221-8686, Japan, ²⁰Faculty of Science and Technology, Graduate School of Science and Technology, Hirosaki University, 3, Bunkyo, Hirosaki, Aomori 036-8561, Japan, ²¹Yukawa Institute for Theoretical Physics, Kyoto University, Kitashirakawa Oiwakecho, Sakyo, Kyoto 606-8502, Japan, ²²Department of Electronic Information Systems, Shibaura Institute of Technology, 307 Fukasaku, Minuma, Saitama 337-8570, Japan, ²³School of Advanced Science and Engineering, Waseda University, 3-4-1 Okubo, Shinjuku, Tokyo 169-8555, Japan, ²⁴National Institute of Polar Research, 10-3, Midori-cho, Tachikawa, Tokyo 190-8518, Japan, ²⁵Faculty of Engineering, Division of Intelligent Systems Engineering, Yokohama National University, 79-5 Tokiwadai, Hodogaya, Yokohama 240-8501, Japan, ²⁶Faculty of Science, Shinshu University, 3-1-1 Asahi, Matsumoto, Nagano 390-8621, Japan, ²⁷Hakubi Center, Kyoto University, Yoshida Honmachi, Sakyo-ku, Kyoto 606-8501, Japan, ²⁸Department of Astronomy, Graduate School of Science, Kyoto University, Kitashirakawa Oiwake-cho, Sakyo-ku, Kyoto 606-8502, Japan, ²⁹Institute of Particle and Nuclear Studies, High Energy Accelerator Research Organization, 1-1 Oho, Tsukuba, Ibaraki 305-0801, Japan, ³⁰University of Pisa, Polo Fibonacci, Largo B. Pontecorvo, 3, 56127 Pisa, Italy, ³¹Astroparticle Physics Laboratory, NASA/GSFC, Greenbelt, Maryland 20771, USA, ³²Department of Electrical and Electronic Systems Engineering, National Institute of Technology, Ibaraki College, 866 Nakane, Hitachinaka, Ibaraki 312-8508, Japan, ³³Department of Astronomy, University of Maryland, College Park, Maryland 20742, USA, ³⁴Department of Physical Sciences, College of Science and Engineering, Ritsumeikan University, Shiga 525-8577, Japan, ³⁵Faculty of Science and Engineering, Global Center for Science and Engineering, Waseda University, 3-4-1 Okubo, Shinjuku, Tokyo 169-8555, Japan, ³⁶Department of Physics and Astronomy, University of Denver, Physics Building, Room 211, 2112 East Wesley Avenue, Denver, Colorado 80208-6900, USA, ³⁷Quantum ICT Advanced Development Center, National Institute of Information and Communications Technology, 4-2-1 Nukui-Kitamachi, Koganei, Tokyo 184-8795, Japan, ³⁸College of Science and Engineering, Department of Physics and Mathematics, Aoyama Gakuin University, 5-10-1 Fuchinobe, Chuo, Sagami-hara, Kanagawa 252-5258, Japan, ³⁹College of Industrial Technology, Nihon University, 1-2-1 Izumi, Narashino, Chiba 275-8575, Japan, ⁴⁰RIKEN, 2-1 Hirosawa, Wako, Saitama 351-0198, Japan, ⁴¹Division of Mathematics and Physics, Graduate School of Science, Osaka City University, 3-3-138 Sugimoto, Sumiyoshi, Osaka 558-8585, Japan, ⁴²National Institutes for Quantum and Radiation Science and Technology, 4-9-1 Anagawa, Inage, Chiba 263-8555, Japan, ⁴³Nagoya University, Furo, Chikusa, Nagoya 464-8601, Japan, ⁴⁴College of Science, Ibaraki University, 2-1-1 Bunkyo, Mito, Ibaraki 310-8512, Japan